Optofluidic Intracavity Spectroscopy of Canine Hemangiosarcoma

Weina Wang, David W. Kisker, Douglas H. Thamm, Hua Shao and Kevin L. Lear, *Member, IEEE*

***Abstract*- The label-free technique of optofluidic intracavity spectroscopy (OFIS) uses light transmitted through a cellular body in a microfluidic optical resonator to distinguish different types of cells by their optical properties. The OFIS technique has differentiated canine hemangiosarcoma (HSA) cell lines from monocytes in peripheral blood mononuclear cells (PBMCs) based on their distinctive transmission spectra. A single characteristic parameter indicative of strong multi-transverse-mode resonances was determined for each cell by forming a linear combination of the mean and standard deviation of the transmission spectra over one free spectral range excluding the peaks of passive Fabry-Pérot cavities without cells. The difference in the characteristic parameters of HSA and monocyte samples was highly statistically significant with a *p*-value as low as 10^{-6}. The same method shows that the characteristic parameters of canine lymphoma and lymphocytes are distinct with a $p < 0.005$. A receiver operating characteristic (ROC) curve constructed from *t*-distributions fit to the HSA and monocytes indicates that 95% sensitivity and 98% specificity can be simultaneously achieved.**

***Index Terms*— biophotonics, optofluidic intracavity spectroscopy, optical cancer diagnostics, transmission parameters, hemangiosarcoma**

I. Introduction

Label-free optical diagnostics offer a variety of advantages and can provide valuable information about the biological state of cells and in particular may be used for cancer detection. Non-destructive and non-chemical optical methods allow reduced test complexity and cost. Optical processes such as absorption, scattering, diffraction and refraction can probe the inherent refractive index properties of cells, which are related to a cell's size, shape and intracellular components. Such cellular morphology information can be used to deduce the biological state of cells [1], including cancer.

Both flow cytometry and, with greater precision, interferometry provide quantitative indications of cellular refractive index. Flow cytometry uses light scattering to infer cell size and granularity information, but it typically employs fluorescent labels in classifying cell types or states. Flow cytometry is a relatively expensive approach and does not measure refractive index with high accuracy. Interferometry is often a preferred technique to obtain information on the refractive index profile and size of objects.

A recent example of optical interferometry of cells involves placing individual cells in laser or resonant cavities and observing how the cells modify the cavity modes. In the majority of previously reported Fabry-Pérot (F-P) cavity based sensing devices, only changes in longitudinal modes were considered. Although the techniques could successfully determine the refractive index and thus infer some information about the biological state of living cells in real time without any cell labeling or chemical treatment, they had some limitations. Gourley et al. [2] first investigated intracavity spectroscopy of cells by developing the biocavity laser, a photopumped vertical external cavity surface emitting laser that combined a microfluidic chamber and a semiconductor gain region. Spectroscopy on spheres and cells were reported using this technique. However, the biocavity laser system required an external laser, which increased the cost of the system and was an impediment to miniaturization. Gourley and co-workers relied on both fundamental mode shifts and observations of the number of transverse modes to characterize cells [3].

Most other microcavity interferometry investigations of cells avoided the complexities of placing them in laser resonators but did not utilize information from transverse mode structure. For example, a microfluidic resonator designed by Domachuk [4] integrated a F-P cavity formed between optical fiber Bragg grating reflectors across a planar microfluidic channel. The position of the phase reflection plane of distributed Bragg reflectors, which was several periods out from the fiber faces [5], made the effective cavity length substantially longer than the channel width, reducing the sensitivity to cellular refractive index. Refractive index changes as low as 0.2% were resolved; however, this approach required sophisticated equipment such as a high-resolution

Manuscript received April 26, 2009.

W. Wang and H. Shao are with the Dept of Electrical and Computer Engineering, Colorado State University, 80523, USA.

D. W. Kisker is with Eoptra, LLC.

D. H. Thamm is with the Dept of Clinical Sciences and School of Biomedical Engineering,, Colorado State University, 80523, USA.

K. L. Lear is with the Dept of Electrical and Computer Engineering and School of Biomedical Engineering, Colorado State University, 80523, USA. (e-mail: kevin.lear@colostate.edu, tel: 970-491-0718).

spectrometer to monitor small shifts in the resonant wavelength of the high finesse cavity. A related on-chip F-P approach demonstrated by Song [6] consisted of a similar passive horizontal cavity formed by coating gold on the facets of single-mode fibers on opposite walls of a microfluidic channel and a micropipette that held a cell. With this device, both the size and refractive index of cells were measured with 0.1% accuracy by altering the index of the fluid around the cell. Even higher cavity finesse was realized due to the shorter effective cavity length between the facets of the fibers, but a high-resolution spectrometer was still an essential part of the apparatus. Transverse mode spectra were not investigated in either one of these fiber-based F-P interferometers, nor did they consider lateral confinement effects.

The optofluidic intracavity spectroscopy (OFIS) technique utilizes optical refraction and diffraction effects in a microfluidic cavity to produce characteristic intracavity transmission spectra of single biological cells in a microscale optical resonator. One goal of the technique is employing the resulting spectra to differentiate cells including distinguishing neoplastic and non-neoplastic cells. As an initial investigation, the OFIS spectra of small numbers of red and white blood and yeast cells as well as microspheres were previously published along with a cross-correlation analysis that indicated some, but not all of the non-cancerous cell types could be distinguished [7]. Subsequently, differentiation of canine lymphoma and lymphocytes with OFIS was successfully demonstrated, and analyzed in terms of longitudinal mode shift and lateral confinement induced by the cells [8].

While that study found mode shifts of canine lymphoma were extremely repeatable, further experiments revealed they were not sufficiently repeatable to distinguish a more aggressive canine cancer cell line, hemangiosarcoma (HSA), from a background of peripheral blood mononuclear cells (PBMCs). Accordingly, this paper presents for the first time an alternative analysis of OFIS spectra based on a single parameter quantification of the strength of transverse modes. The authors demonstrate in this work that the method is applicable to both HSA and canine lymphoma and believe it may be more generally applicable to a wide range of cancers including human ovarian and pancreatic as will be published elsewhere.

The two types of cancer cells used in this research, HSA and lymphoma, are two of the most common canine cancers. Although extremely rare in humans, canine HSA is a common disease, typified by rapid and widespread metastasis, and a very poor prognosis [9], for hardly any symptoms exhibit until an advanced stage when treatment is usually unsuccessful. Novel techniques for its early detection would be of considerable clinical utility since early stage diagnosis may offer better treatment alternatives. Canine lymphoma histologically resembles human intermediate- to high-grade non-Hodgkin's lymphoma [10], and is typified by very similar biologic behavior and response to therapy. Currently the only clinically accepted diagnostic tool for HSA detection is tumor biopsy at advanced stages. Modiano and co-workers have investigated the use of flow cytometry incorporating up to 6 fluorescent labels and concluded that this technique may be useful in HSA diagnosis [11]. However, their research requires additional confirmation, and the relatively high cost of flow cytometery equipment and supplies and necessary operational expertise would limit access to this technique as reflected by the fact that only four veterinary hospitals in the U.S. are known to include flow cytometry labs. The need to rapidly and economically diagnose HSA with extremely poor prognosis from operable benign tumors in dogs with internal bleeding motivates research on low cost, widely available diagnostics for this disease.

The remainder of the paper is organized to sequentially present experimental methods, resulting spectra, data analysis, and conclusions. After briefly reviewing the OFIS operating concept, Section II describes the apparatus and procedures for cell preparation, spectral measurements, and data normalization. Section III offers typical spectra for two cancer cell lines, canine lymphoma and HSA, that display multiple transverse modes and two non-cancerous types of leukocytes, lymphocytes and monocytes, that do not contain transverse modes. Data analysis in Section IV relies on the new method of parameterizing transverse mode strength to distinguish cancerous cells. Statistical analysis shows that the new method to parameterize HSA and monocyte transverse mode spectra can properly categorize the cells with good sensitivity and specificity. A receiver operating characteristic (ROC) curve is presented in Section IV. Earlier publications on OFIS [7, 8] and the other microcavity techniques referenced above [4, 6] have not presented statistical analysis on multiple cells, such as sensitivities, specificities, nor ROC curves.

II. Experimental Methods

A. Detection mechanism of OFIS

The resonant cavity used in OFIS is a F-P cavity formed by two plane mirrors above and below a microfluidic channel, and the cavity's resonant modes are determined by its length and the media inside. A F-P cavity filled with media of homogenous refractive index n exhibits transmission peaks at each wavelength that fits into the cavity an integer number of times, $\lambda_0 = 2nL_{cav}/m$, where λ_0 is the optical wavelength in air, L_{cav} is the cavity length and m is the integer longitudinal mode order. These modes are affected by the refractive index in the longitudinal direction of the cavity and are spaced by the cavity's free spectral range (FSR), a property of a cavity that is determined by its length and refractive index according to $FSR=\lambda_0^2/2nL_{cav}$. The peaks of a bare cavity's transmission spectrum, such as those shown in Fig. 1, correspond to its resonant wavelengths.

Placing an object with a different refractive index than the surrounding media in a F-P cavity alters its resonant mode wavelengths due to the local index change. When the cavity is loaded with material that has higher refractive index than that of the cavity, such as a cell that has a higher index than the surrounding fluid, the length of optical path in the longitudinal direction will increase, causing the resonant transmission peaks to shift to the longer wavelengths. In addition, the cell's lateral index profile will induce transverse variation of the optical field distribution in directions parallel to the mirrors [8]. Each self-consistent transverse field distribution will

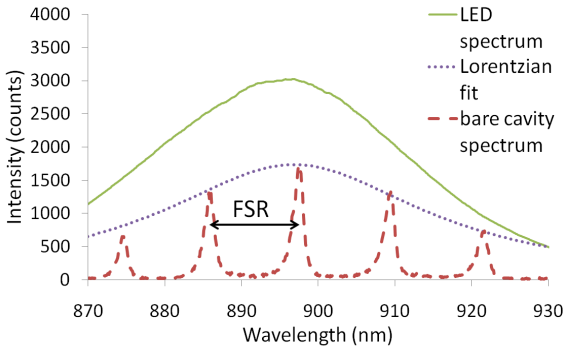

Fig.1. LED (solid) and bare cavity spectra (dashed) with Lorentzian fit (dotted).

create an additional transmission peak that is shifted from the transmission peak wavelength that would result from a change in the longitudinal optical path length alone. Hence a cell's index profile will affect the number, position, and magnitude of transmission peaks corresponding to multiple transverse modes that occur between adjacent longitudinal modes. The set of transverse modes occurring between neighboring longitudinal modes, i.e. over one FSR, are termed a transverse mode group, and the transverse mode group is repeated for each longitudinal mode [12]. Combined, the wavelength shift and the number, position, and magnitude of transverse modes in the transmission spectrum can be used to infer refractive index information about the cell, which is a function of its size, shape, and intracellular components (such as nuclear and cytoplasm sizes and refractive index), and this information can be used to measure the biological state of a cell [13].

B. Chip fabrication and spectral data acquisition

Cells were delivered to a microfluidic F-P cavity on OFIS chips, where the transmission spectrum of the cell-loaded cavity was collected. Compared to the OFIS chip fabrication reported in [8], the process was further optimized and simplified. Low temperature epoxy bonding, instead of thermal bonding, was applied to seal the mirror coated substrate and superstrate together. The cavity depth was primarily determined by the etch depth in the substrate, with only a minor contribution from the thin epoxy layer. Before the epoxy cured, the planarity of the mirrors was examined to ensure good optical performance of the chip. The schematic diagram of OFIS chip is shown in Fig.2.

To acquire transmission spectra an OFIS system [7, 8, 14] as illustrated in Fig.3 was used. An infrared LED was focused to increase incident intensity, but the extended nature of the LED source still illuminated a large area on the chip. However, the approximately 10 µm diameter image of the fiber core, comparable with the size of a single cell, acted as a spatial filter in the plane of the chip, sampling the spectra only from that limited area. The 5× objective's numerical aperture (N.A.) of 0.1 was smaller than the illumination cone and determined the range of incident angles that were sampled. Temporary back illumination through the fiber was used to focus the core image on the chip and to find the corresponding location on the camera display, which was noted and served as the light collection spot when acquiring spectra. Once the cells temporarily settled on the channel bottom, in-plane translation of the chip was used to align the collection spot to individual cells. Associated bare cavity reference spectra were either

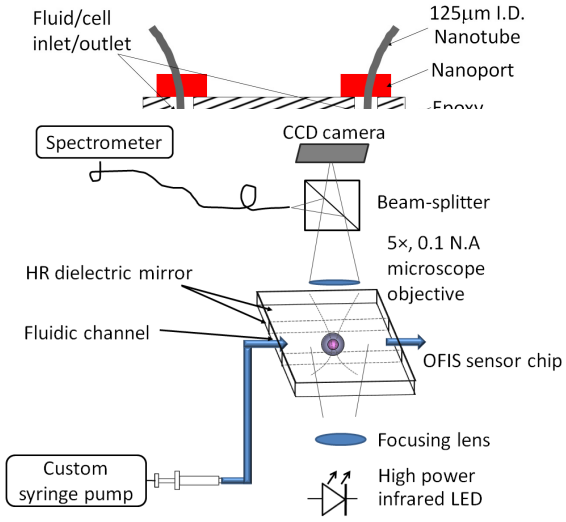

Fig.3. OFIS system apparatus.

taken by translating the cell just out of the collection spot or by temporarily increasing flow rate to push the cell away from the spot. Each spectrum of an individual cell and the corresponding bare cavity spectrum were obtained with the same integration time, typically 3 to 6 seconds to achieve sufficient signal-to-noise ratio for the data acquired from different cavities.

C. Flow control

Fluids and cells were delivered to the chip by pressure driven flow from a custom syringe pump through nanotubes (PEEK T-1576, Upchurch Scientific) and nanoport assemblies illustrated in Fig.2. Conventional pressure driven flow would result in excessive flow velocities of over 1000 µm/sec and might cause clogging at the beginning the microfluidic channel, where the cross-section area was greatly reduced from the 1mm diameter inlet to the 200 µm wide channel. To avoid clogging, low flowrate was achieved at the beginning of each experiment by running the syringe pump with a small duty cycle, typically 10%. Steady flow was observed under pulsed drive conditions due to compressible air space in the syringe combined with the low conductance of the nanotube and microchannel acting as a low pass mechanical frequency filter. After flowing cell suspensions through the nanotube into the channel, the syringe pump was stopped and manual control of the syringe was used to further slow down the flowrate, until minimal velocity was achieved and some cells temporarily settled on the channel bottom. Other cell immobilization methods, such as dielectrophoresis, are under investigation and will be integrated in the OFIS system in the future. Although a short channel was preferred for the stability of optical resonators [7], it was more readily clogged by cells, especially when their size was comparable to the channel depth, such as HSA cells in the 16 µm deep channel.

D. Raw spectrum normalization

To obtain the spectral transmission of the cavities, raw spectral data were normalized using a unity transmission spectrum. Bare cavity spectra, such as the one shown by the dashed line in Fig. 1, contained only longitudinal peaks separated by a FSR. The envelope of the peaks was approximately, but not exactly proportional to the LED spectrum, also seen in Fig. 1, due to other optical effects. To properly normalize the cell transmission spectra, the peaks of the bare cavity spectra were assumed to represent unity transmission of the F-P cavity since the reflectivity of the two mirrors was nominally matched. The peaks in the 880 to 920 nm range of a bare cavity spectrum collected from a location next to each cell was fit to a Lorentzian line shape, illustrated by the dotted curve in Fig 1, by adjusting the fit's peak wavelength, peak height, peak width and a small skew factor if necessary. The intensity of the Lorentzian curve was then taken to represent unity transmission for the corresponding cell spectrum to allow normalization of spectral regions between the bare cavity peaks. The statistical significance of the results, i.e. *p*-values reported in Section IV, was nearly independent of the exact parameters of the unity transmission fit and even the functional form of the fit.

E. Cell sample preparation

Optical properties of one HSA cell line, DEN-HSA and two lymphoma cell lines, OSW and 1771 were investigated with the OFIS technique. The DEN-HSA canine HSA cells were established in the laboratory of Thamm et al. [15], and the OSW canine T-cell lymphoma cells were provided by Dr. W. Kisseberth, Ohio State University [16]. The 1771 canine B-cell lymphoma cell line was provided by Dr. K.A. Jeglum, Wistar Institute [17, 18, 19].

Cells were cultured in minimal essential medium (MEM, BioWhittaker, Walkersville, MD) supplemented with 10% heat inactivated fetal bovine serum (HyClone, Logan, UT), 100 units/ml penicillin–streptomycin (Mediatech, Herndon, VA), 2 mM L-Glutamine (Mediatech), 1 mM sodium pyruvate (Mediatech) and 1X nonessential amino acid solution (Sigma, St. Louis, MO)(C/10%), at 37°C, 5% CO_2 in a humidified atmosphere, and suspended in C/10% on ice prior to utilization in the described experiments. Fig. 4 shows microscopic images of individual stained monocyte and HSA cells from cytospin slides. Monocytes, lymphocytes, and a small fraction of neutrophil granulocytes were found in the PBMC samples. Monocytes were manually selected during collection of OFIS transmission spectra of unstained PMBC based on obvious size differences between the monocytes (approximately 14-17 μm), lymphocytes (7-8 μm) and neutrophil granulocytes (10-12 μm) [20]. The spectra of the smaller PBMCs were observed to be less likely to contain any observable peaks away from the bare cavity modes.

III. Experimental Results

A. HSA and monocyte results

Transmission spectra of neoplastic and non-neoplastic cells

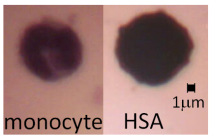

Fig. 4. Microscopic images of cytospin slides of stained monocytes in PBMC and HSA cells under 40× magnification.

were collected with OFIS chips of different cavity depths. Cavity depths were determined from the FSR of the transmission spectra collected from fluid-filled bare cavities. Three separate chips with cavity depths of 16, 22, and 25 μm were used to measure transmission spectra of HSA cells; and the 22 μm and 25 μm channel were then used to take transmission spectrum of baseline monocytes. Earlier studies on lymphoma and lymphocytes used a separate 15.8 μm deep channel [8].

Transmission spectra of 24 unstained single cells from the canine DEN-HSA cell line and 24 unstained baseline normal monocytes were collected and analyzed. Example normalized transmission spectra of cells in a 25 μm deep cavity are plotted in Fig. 5, where vertical lines on each spectrum mark the peak wavelengths of the bare cavity taken at the same location as each cell or immediately adjacent to it. The exact wavelength of the bare cavity modes acquired in conjunction with cells at different positions along the channel shifted due to changes as small as 0.2% in the cavity length. However, the absolute wavelengths of the spectral peaks are not important for the new detection method presented in Section IV. Since the cells were settled on the bottom of the channel

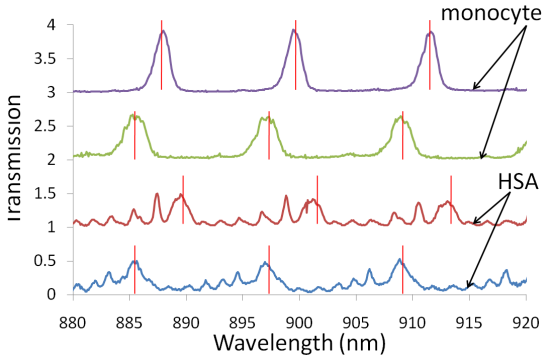

Fig.5. Normalized transmission spectra of HSA cells and monocytes collected from a 25 μm deep channel. Vertical lines indicate the bare cavity modes at the same or adjacent location for each cell. Each spectrum is offset from the one below it by one unit on the transmission scale.

rather than rotating, each cell's spectra was relatively constant.

Although the HSA spectra were acquired from two different cavities, the absolute cavity length is not a critical parameter of the intracavity spectroscopy. In both 25 μm and 22 μm cavities, monocytes and HSA cells showed distinctively different spectral characteristics. The spectra of the non-neoplastic monocytes were dominated by peaks near the bare cavity mode positions with only very weak intervening modes. In contrast, the majority of HSA cells exhibited several well-defined, significant transverse modes of moderately uniform spacing and weakened peaks near the bare cavity mode wavelengths. Transverse mode groups were repeated for each longitudinal mode and were spaced by the cavity's FSR of approximately 12 nm or 14 nm, corresponding to a cavity length of 25 μm and 22 μm, respectively.

B. *Lymphoma and lymphocyte results*

The distinctive spectral properties of canine lymphoma and lymphocytes were previously reported [8]. Lymphocytes were used as a control for the two lymphoma cell lines that were investigated, OSW and 1771. Fig.6 shows typical lymphoma and lymphocyte spectra from a 15.8 μm deep cavity used in that study, and the vertical lines on each spectrum marked the peaks of bare cavity modes as noted above.

Lymphoma cells from both cell lines exhibited multi-mode behavior with at least two clear transmission peaks in each free spectral range. The primary peak, attributed to the fundamental mode, was well separated from the bare cavity resonance obtained at the test locations adjacent to each cell. The measured fundamental mode wavelength shifts were extremely repeatable for different lymphoma cells from the same cell line with a standard deviation of ±0.13 nm. The lymphocyte control spectra had a fundamental mode as well, but no higher order transverse modes were observed for these non-neoplastic cells. The lymphocytes also exhibited very repeatable wavelength shifts. However, the wavelength shifts of the HSA spectra were much more widely distributed, potentially indicating a wider variation in cell or nucleus size due to the more aggressive nature of HSA and corresponding rapid progression through the cell cycle.

Due to the variability in wavelength shifts for HSA, the method investigated for discrimination of lymphoma and lymphocyte spectra was not directly useful for HSA and monocyte spectra, motivating a different analysis approach. The method presented in Section IV utilized the average transmission and standard deviation of transmission computed from each cell's transmission spectrum to compare different cell types and distinguish them. As discussed below, the new method worked well for both types of canine cancer.

IV. Data Analysis

A. *Transmission parameters method*

Qualitative observation of the HSA spectra in Fig. 5 and the lymphoma spectra in Fig. 6 indicates that these cancer cell lines produce much stronger transverse mode peaks between the bare cavity modes than the corresponding monocyte and lymphocyte controls. Even in the absence of a precise physical model, the differences motivate an effort to quantify the strength of transverse modes away from the bare cavity peaks and seek a correlation of the transverse mode strength parameters with a binary categorization of cells as neoplastic or non-neoplastic. Two quantitative measures of the strength of transverse modes were analyzed. One is the mean value of transmission, T, and the other is the standard deviation of the transmission, σ_T. Casual observation suggests the presence of multiple transverse modes is correlated with neoplastic cells. To quantify the extent of multimode spectra, it is noted that well-defined transverse mode peaks that have significant peak transmission height will produce a larger mean value of transmission and generally a larger fringe modulation depth. However, if the individual transverse modes for HSA are not well resolved due to the increase of background noise, the mean transmission would increase, but the standard deviation value would be diminished. Also, neoplastic cells that produced low intensity transmission peaks with large fringe depth were sometimes observed where, although the resulting mean transmission is low, the standard deviation value is comparable with that of other neoplastic cells. Hence, both the mean transmission and standard deviation of the transmission were considered.

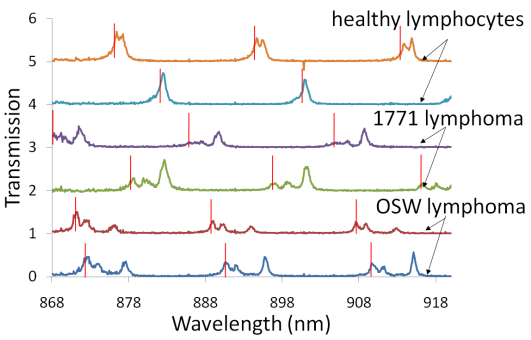

Fig.6. Normalized transmission spectra of healthy canine lymphocytes and neoplastic lymphoma cells from two different cell lines, OSW and 1771. Vertical lines indicate the bare cavity mode wavelengths adjacent to each cell.

The two parameters, T and σ_T, of the normalized transmission spectra (using the normalization method described in Section II. D) of all 16 HSA cells and 16 monocytes in the 25 μm deep channel, and all 8 HSA and 8 monocytes in the 22 μm deep channel were computed and plotted in Fig. 7. To prevent the bare cavity modes from influencing the parameters, the calculations were performed only on data at least one full-width-at-half-maximum (FWHM) away from the adjacent bare cavity mode peaks.

In the scatter plot, the neoplastic and non-neoplastic cells in both channels are divided into two groups. In comparison to the monocyte spectra, HSA cell spectra have a higher mean transmission value, and are more likely to have a greater transmission standard deviation, indicating HSA has stronger transverse modes that are attributed to the enlarged nucleus of neoplastic cells. Large standard deviation of transmission values indicate large differences between transmission peaks and valleys, i.e. greater contrast, but do not indicate a lack of repeatability in individual cell spectra.

To support the generality of this method, it was also applied to previously reported lymphoma and lymphocyte results acquired in a 15.8 μm deep channel with the OFIS technique. Although the number of cells being interrogated was more limited, the neoplastic lymphoma and non-neoplastic lymphocyte were divided into two groups as well, as shown in Fig. 8.

B. *Statistical Analysis and Significance*

A statistical hypothesis test, Student's *t*-test was applied to evaluate the difference in transmission parameters of neoplastic and non-neoplastic cells. To assess potential clinical significance, the sensitivity and specificity for detecting neoplastic cells was evaluated by constructing a receiver operating characteristic (ROC) curve. Typical ROC curves are generated by varying the classification threshold with respect to a single parameter. In order to form a single parameter for classification, a weighted sum of the mean and standard deviation of the transmission $W_T = kT + \sigma_T$ was used, where k is a constant chosen to roughly optimize statistical

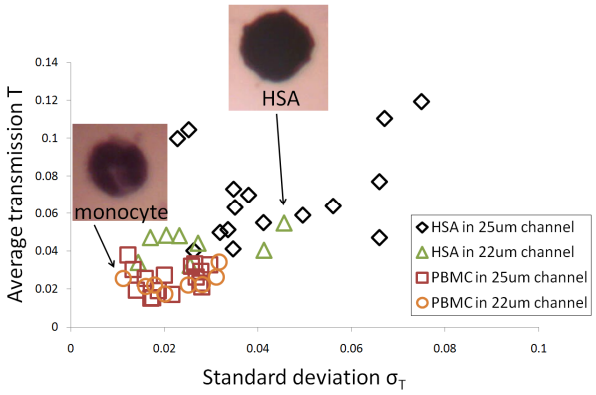

Fig.7. Scatter plot of transmission results of HSA and monocytes in 25 µm and 22 µm deep channels.

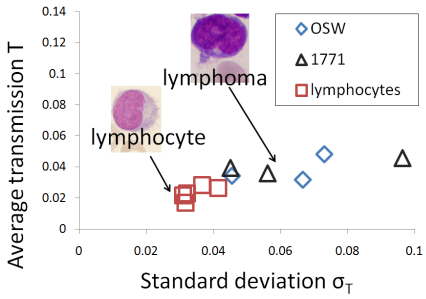

Fig.8. Scatter plot of transmission results of lymphoma and lymphocyte; inset reproduced with permisson from Lymphomas Extensive Image Collection © 2009 Rector and Visitors of the University of Virginia, Charles E. Hess, M.D. and Lindsey Krstic, B.A.

significance of the data sets reported in this paper. The distinctiveness of the cell populations varied weakly but smoothly with k. This single combined transmission parameter enabled quantitative analysis of the transmission spectrum of any individual cell, and a two sample Student's t-test [21] was carried out to verify the statistical importance of neoplastic and non-neoplastic cell classification.

For the HSA and monocyte transmission collected from the 25 µm deep channel with k = 2, the standardized variable (t-score) between the two samples was 7.45, and the number of degrees of freedom from the total of 32 samples was 17, resulting in a p-value of 1.0×10^{-6}. For the cell transmission collected from the 22 µm deep channel, the t-score was 4.63, and the number of degrees of freedom from the total of 16 samples was 12, resulting in a p-value of 5.8×10^{-4}. The very small p-values show that the classification of HSA and monocyte had extremely high statistical significance.

To further validate the general applicability of using the weighted sum of transmission parameters, W_T, to differentiate neoplastic and healthy cells, it was applied to the previously reported lymphoma and lymphocyte transmission spectra [8]. The resulting t-score between the two cell types was 4.59 and the number of degrees of freedom from the total of 11 samples was 6. The small sample size produced a somewhat higher, but still quite small null hypothesis probability of $p = 3.8\times10^{-3}$. In comparison, the peak shifts for lymphoma and lymphocytes were extraordinarily well separated. The peak shift mean values and standard deviations reported in Reference 7 of 20.38 ± 0.30 nm for 10 lymphocytes and 24.59 ± 0.13 nm for 10 OSW lymphoma cells yielded a t-score of 40.7. While these data indicate that a weighted transmission parameter is not the optimum approach for distinguishing lymphoma and lymphocytes based on the prior data, the p-values of < 0.005 for HSA in two different cavity lengths as well as lymphoma suggests the new approach may be broadly applicable for detecting multiple types of cancer cells.

C. *ROC curve*

For a preliminary assessment of clinical utility, a ROC curve [22] was generated for HSA cells and monocytes in the 25 µm deep channel. Due to the limited number of samples, t-distributions were fit to W_T values for the two cell types. Note that t-distributions have larger tails than normal distributions, making the use of t-statistics more conservative and leading to slightly lower sensitivity and specificity predictions than normal statistics would. The sample mean ± sample standard deviation for HSA was $W_T = 0.185\pm0.058$, while the monocyte distribution produced $W_T = 0.072\pm0.016$. Numerical integration of the t-distributions as the classification threshold was varied produced the most probable ROC curve as shown by the solid line in Fig. 9 [23]. Upper and lower 95% confidence limits on the ROC curve, shown with dashed lines, were computed by shifting the t-distribution mean values for HSA and monocytes in opposite directions by 2.14 times the standard deviations of the sample means. Moving the mean values toward each other gave a lower 95% confidence limit on the ROC curve while shifting them farther apart generated the upper 95% confidence limit on the curve. The small sample size necessitated the use of t-distributions to construct a reasonable ROC curve as the 25 µm deep channel provided perfect separation of the HSA and monocyte samples with a classification threshold $W_T = 0.1$. While t-distributions are more conservative than normal distributions, deviations of the transmission parameters of biological cells from either distribution are possible, particularly in the tails. Such deviations would alter the exact locus of the ROC curve [24].

The most probable ROC curve indicated that a diagnostic or screening test for individual HSA cells based on OFIS transmission parameters could simultaneously offer 95% sensitivity and 98% specificity. To quantitatively estimate the accuracy of an OFIS based HSA diagnostic test [22, 25], the area under the ROC curve (AUC) was computed to be 0.981+0.014/-0.046 with 95% confidence limits. A diagnostic test is considered "very good" if the AUC is between 0.92 and 0.97 [26], and the full 95% confidence band falls well within or above this range. Similar ROC curve generated for the HSA and monocytes in the 22 µm deep channel indicated 91% sensitivity and 94% specificity, with AUC of 0.961. The absolute channel depth is not a critical parameter of the OFIS diagnostic tool.

Although the mode shift method [8] is no longer suitable for the analysis of HSA spectra, the transmission parameters method applied here was proven to have sufficient sensitivity and specificity to differentiate neoplastic and non-neoplastic cells, such as canine HSA and monocyte. The generality of this method was further supported by discriminating canine lymphoma and lymphocyte.

V. Conclusion

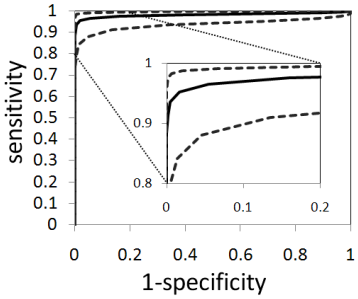

Fig.9. ROC curve of HSA detection against monocytes, with inset enlarging the top left corner of the ROC curve.

OFIS sensor chips combine microfluidic cell handling and a F-P cavity to acquire transmission spectra that are qualitatively and quantitatively different for neoplastic and non-neoplastic cells. Neoplastic cells produce multimode transmission spectra while non-neoplastic cells create only weak transmission peaks between bare cavity modes. When parameterized with a linear combination of average transmission and the standard deviation of transmission, the spectra of HSA cells and monocytes in canine PBMCs were found to be distinct with extremely high statistical significance ($p < 10^{-6}$ to 10^{-3}). Statistically distinct distributions of one single number that quantitatively summarize the transmission of the transverse modes, the weighted transmission parameters, were also obtained for canine lymphoma and lymphocytes although the separations in the populations were not as extreme as found for peak wavelength shifts from the same cells. An ROC curve indicated that excellent sensitivity and specificity could be obtained for an individual HSA cell diagnostic test using the new method; and this classification result is not significantly dependent of cavity length.

OFIS may be a useful tool for early detection of canine cancers including HSA and lymphoma. If the preliminary results reported here can be properly applied, such a diagnostic cancer test based on blood samples could substantially increase survivability of canine cancer patients and provide dog owner with more certain prognosis at reduced cost when facing decisions on treatment of suspected HSA. The extent of circulating HSA cells is presently unknown but speculated to be as high as 1% of the leukocyte count due to the intimate contact between this sarcoma of endothelial blood vessel tissue and the blood stream. Thus HSA detection may be an easier initial application of the OFIS techniques ultimately intended to identify rare circulating tumor cells in humans at a level of only 1 cancer cell per 10^6 or more leukocytes.

In the future, continuing investigation of intracavity spectroscopy of additional types of canine and human cancer are expected to validate the utility of an OFIS diagnostic tool for different kinds of tumor cells. Also, more detailed analysis of the transverse mode spectra from OFIS is likely to reveal greater information about cells including relative refractive index and shape including asymmetry.

ACKNOWLEDGEMENT

The authors thank Barbara Rose at the CSU Animal Cancer Center for her generous help in cell culturing, cytospin slide preparation, and useful discussions. They also thank Ellen Eliason Kisker for the valuable insights on statistical analysis.

REFERENCES

[1] V. Backman, M. B. Wallace, L. T. Perelman et al., "Detection of preinvasive cancer cells," *Nature*, vol. 406, no. 6791, pp. 35-36, Jul, 2000.

[2] P. L. Gourley, A. E. McDonald, and M. F. Gourley, "Vertical cavity surface-emitting laser scanning cytometer for high speed analysis of cells", *SPIE*, vol. 2679, pp. 131-141, 1996.

[3] P. L. Gourley, "Biocavity laser for high-speed cell and tumour biology," *Journal of Physics D-Applied Physics*, vol. 36, no. 14, pp. R228-R239, Jul, 2003.

[4] P. Domachuk, I. C. M. Littler, M. Cronin-Golomb et al., "Compact resonant integrated microfluidic refractometer," *Applied Physics Letters*, vol. 88, no. 9, Feb, 2006.

[5] D. I. Babic, and S. W. Corzine, "Analytic expressions for the reflection delay, penetration depth, and absorptance of quarter-wave dielectric mirrors," *IEEE Journal of Quantum Electronics*, vol. 28, no. 2, pp. 514-524, Feb, 1992.

[6] W. Z. Song, X. M. Zhang, A. Q. Liu et al., "Refractive index measurement of single living cells using on-chip Fabry-Perot cavity," *Applied Physics Letters*, vol. 89, no. 20, Nov, 2006.

[7] H. Shao, D. Kumar, and K. L. Lear, "Single-cell detection using optofluidic intracavity spectroscopy," *IEEE Sensors Journal*, vol. 6, no. 6, pp. 1543-1550, Dec, 2006.

[8] H. Shao, W. Wang, S. E. Lana, and K.L. Lear, "Optofluidic intracavity spectroscopy of canine lymphoma and lymphocytes," *IEEE Photonics Technology Letters*, vol. 20, no. 5-8, pp. 493-495, Mar-Apr, 2008.

[9] D. H. Thamm, "Miscellaneous Tumors: Hemangiosarcoma", in *Withrow and MacEwan's Small Animal Clinical Oncology*, 4th Edition, ed. S. J. Withrow and D. M.Vail, , Philadelphia: W.B. Saunders, 2007. 785-795.

[10] R. M. Jacobs, J. B. Messick, and V. E. O. Tumors of the hemolymphatic system. In: Meuten DJ (ed). *Tumors in Domestic Animals*. 4th Ed. Ames (IA): Iowa State Press; 2002:119-198.

[11] A. R. Lamerato-Kozicki, K. M. Helm, C. M. Jubala et al., "Canine hemangiosarcoma originates from hematopoietic precursors with potential for endothelial differentiation," Experimental Hematology, vol. 34, no. 7, pp. 870-878, Jul, 2006.

[12] A. E. Siegman, *Lasers*. Mill Valley, CA: University Science, 1986, Chapter 19.

[13] J. Beuthan, O. Minet, J. Helfmann, M. Herrig, and G. Muller, "The spatial variation of the refractive index in biological cells," *Physics. in Medicine and Biology*, 41 (1996) 369.

[14] H. Shao, D. Kumar, S. A. Feld, and K.L. Lear, "Fabrication of a Fabry-Perot cavity in a microfluidic channel using thermocompressive gold bonding of glass substrates," *Journal of Microelectromechanical Systems*, vol. 14, no. 4, pp. 756-762, Aug, 2005.

[15] D. H. Thamm, E. B. Dickerson, N. Akhtar et al., "Biological and molecular characterization of a canine hemangiosarcoma-derived cell line," *Research in Veterinary Science*, vol. 81, no. 1, pp. 76-86, Aug, 2006.

[16] W. C. Kisseberth, M. V. P. Nadella, M. Breen et al., "A novel canine lymphoma cell line: A translational and comparative model for lymphoma research," *Leukemia Research*, vol. 31, no. 12, pp. 1709-1720, Dec, 2007.

[17] C. Rosales, K. A. Jeglum, M. Obrocka et al., "Cytolytic activity of murine anti-dog lymphoma monoclonal-antibodies with canine effector-cells and complement," *Cellular Immunology*, vol. 115, no. 2, pp. 420-428, Sep, 1988.

[18] Z. Steplewski, C. Rosales, K. A. Jeglum et al., "In vivo destruction of canine lymphoma mediated by murine monoclonal antibodies," *In Vivo*, 4(4): p. 231-4, 1990.

[19] S. E. Suter, M. B. Chein, V. von Messling et al., "In vitro canine distemper virus infection of canine lymphoid cells: A prelude to oncolytic therapy for lymphoma," *Clinical Cancer Research*, vol. 11, no. 4, pp. 1579-1587, Feb, 2005.

[20] Daniels, Victor G.; Wheater, Paul R.; Burkitt, H. George (1979). *Functional histology: a text and colour atlas*. Edinburgh: Churchill Livingstone.

[21] Jay. L. Devore, *Probability and Statistics for Engineering and the Sciences*, Thomson Brookes/Cole, 6th edition, 360-373

[22] K. H. Zou, A. J. O'Malley, and L. Mauri, "Receiver-operating characteristic analysis for evaluating diagnostic tests and predictive models," *Circulation*, vol. 115, no. 5, pp. 654-657, Feb, 2007.

[23] T. Fawcett, "An introduction to ROC analysis," *Pattern Recognition Letters*, vol. 27, no. 8, pp. 861-874, Jun, 2006.

[24] Margaret Sullivan Pepe, "*The Statistical Evaluation of Medical Tests for Classification and Prediction*," Oxford University Press, USA; 1st edition ,May 2003
[25] J. A. Hanley, and B. J. McNeil, "The meaning and use of the area under a receiver operating characteristic (ROC) curve," *Radiology*, vol. 143, no. 1, pp. 29-36, 1982.
[26] P. H. Brubaker, "Do Not Be Statistically Cenophobic TIME TO ROC AND ROLL!" *Journal of Cardiopulmonary Rehabilitation and Prevention*, vol. 28, no. 6, pp. 420-421, Nov-Dec, 2008.

Weina Wang received the B.S. degree in Opto-Electronics from Tsinghua University, Beijing, China in 2004 and the M.S. degree in Micro-Electronics from University of Southampton, Southampton, UK in 2006.

She is working toward the Ph.D. degree in Electrical and Computer Engineering at Colorado State University, Fort Collins, US, since August 2006. Her research interests include the design and fabrication of optical biosensors and optical modeling of single cell sensing structures.

Ms. Wang is a student member of SPIE and received a Research Excellence Award for her work in 2010.

Dr. David W. Kisker received the B.A. degree from Rice University in 1974, and a Ph.D. from Stanford University in 1981. He was a Member of Technical Staff at AT&T Bell Laboratories from 1983 until 1990 and a Research Staff Member at IBM T.J. Watson Research Center in Yorktown Heights, NY until 1998. From 1998 to 1999, he was the Director of VCSEL Technology Development at Cielo Communications and VP of Technology Development from 1999 until 2002. From 2002 until 2005, Dr. Kisker was Director of Technology Development at the Broomfield, CO facility of Optical Communications Products.

He is a co-founder of eOptra LLC, a small company dedicated to the deployment of optical technologies to applications in the health care field. Dr. Kisker was elected as a Fellow of the American Physical Society for his ground-breaking work on the in-situ characterization of vapor phase epitaxial growth using x-ray scattering.

Dr. Douglas H. Thamm received his B.A. (Biology) and V.M.D. (Veterinary Medicine) degrees from the University of Pennsylvania in 1990 and 1995 respectively. He completed a residency in Oncology and a 2-year postdoctoral fellowship in the laboratory of E. Gregory MacEwen at the University of Wisconsin-Madison from 1996-2001, followed by a 2-year appointment as a research scientist at the University of Wisconsin-Madison. He joined the faculty in the College of Veterinary Medicine and Biomedical Sciences at Colorado State University in 2004.

His research interest centers around the investigation of novel diagnostics and targeted therapeutics for the treatment of canine cancer, and their translational application to the human disease.

Dr. Thamm is a member of the American College of Veterinary Internal Medicine, the Veterinary Cancer Society, and the American Association for Cancer Research.

Dr. Hua Shao received the B.S.E.E. and the M.S. degrees in physics from Nanjing University of Science and Technology, Nanjing, China, in 1998 and 2001, respectively, and the Ph.D.E.E. degree from Colorado State University in 2007. Her research interests include the design and fabrication of photonic biosensors, and numerical modeling of optical waveguides.

From 2007, she joined National Semiconductor Corporation as a senior analog design engineer.

Dr. Kevin L. Lear (SM'88–M'90) received the B.S.E.E. degree from the University of Colorado, Boulder, in 1984 and the M.S.E.E. and Ph.D.E.E. degrees from Stanford University, Stanford, CA, in 1985, and 1990, respectively.

He was a Senior Member of Technical Staff at Sandia National Laboratories, Albuquerque, NM, from 1990 to 1997. In 1997, he became the Chief Scientific Officer at Micro Optical Devices, Inc., Albuquerque: a small business commercializing VCSELs, which was subsequently acquired by Emcore Corporation. In 1999, he joined Colorado State University, Fort Collins, as the Rockwell Anderson Associate Professor of Electrical and Computer Engineering. His research is currently focused on photonic biosensors and components and systems for high-speed optical communication.

Dr. Lear received an IEEE Lasers and Electro-Optics Society Distinguished Lecturer Award in 1996 for his work on VCSELs.